Disruption of Ozone Recovery by Halogen Emissions from a Regional Nuclear Conflict

Simchan Yook[1]*, and Susan Solomon[1]

Affiliations:

[1] Department of Earth, Atmospheric and Planetary Sciences, Massachusetts Institute of Technology, Cambridge, MA, USA

* Corresponding author. Email: syook@mit.edu

Abstract:

The Antarctic ozone hole, first identified in 1985, is primarily caused by human-produced ozone-depleting substances (ODSs). Following the adoption of the Montreal Protocol and the resulting reduction in anthropogenic ODS emissions, consistent signs of gradual ozone recovery have been reported in observations and a wide range of climate model simulations. Model projections suggest that stratospheric ozone will likely fully recover by the late 21st century. Here, using a climate-chemistry model, we first simulate the recovery of the global ozone burden under declining stratospheric chlorine loading. We then examine how a regional nuclear conflict occurring in the late 21st century could substantially reverse this recovery. Nuclear detonations over urban areas are expected to ignite large-scale fires that emit not only soot but also reactive halogen compounds, including chlorine and bromine, released from the burning of urban structures and industrial materials. These emissions, in turn, lead to substantial reductions in global ozone, primarily through heterogeneous chemical reactions involving chlorine and bromine species on the surfaces of smoke particles. These findings suggest that even a regional nuclear conflict would substantially damage the ozone layer, reversing decades of recovery under the Montreal Protocol.

Plain Language Summary:

The Antarctic ozone hole, first discovered in 1985, is caused mainly by human-made chemicals used in products like refrigerators and aerosol sprays. Following the adoption of the Montreal Protocol and the subsequent decline in emissions of these ozone-depleting substances, both observations and climate model simulations have documented gradual ozone recovery, with full recovery of stratospheric ozone projected by the late 21st century. In this study, using a climate-chemistry model, we simulate the trajectory of global ozone recovery under decreasing stratospheric chlorine loading and investigate how a regional nuclear conflict in the late 21st century could significantly affect this ozone recovery. Nuclear detonations over cities would start large-scale fires that emit not only soot but also ozone-destroying halogen compounds, including chlorine and bromine from the burning of urban structures and industrial materials. These emissions drive substantial global ozone depletion, primarily through heterogeneous chemical reactions involving chlorine and bromine species on the surfaces of smoke particles. These findings suggest that even a regional nuclear conflict would substantially damage the ozone layer, reversing decades of recovery under the Montreal Protocol.

Key Points:

- WACCM4 projects ozone recovery to near 1980 levels by the late 21st century as stratospheric chlorine declines under the Montreal Protocol
- A regional nuclear conflict in 2070 could reverse the recovery, driving SH ozone below the 2000–2020 baseline and forming Arctic ozone holes
- Reactive halogen emissions from urban fires drive ozone loss via chlorine- and bromine-catalyzed heterogeneous chemistry on smoke particles

Main Text:

1. Introduction

The Antarctic ozone hole, first discovered in 1985 (Farman et al., 1985), has attracted sustained attention from the scientific community, policymakers, and the public. Its primary cause is anthropogenic emissions of ozone-depleting substances (ODSs; Solomon et al., 1986). Following the phase out of ODS production and consumption under the Montreal Protocol and subsequent amendments, modeling studies projected Antarctic ozone recovery to 1980 levels by around mid-21st century (Dhomse et al., 2018; Eyring et al., 2007; Keeble et al., 2021; Newman, 2018). Ozone healing has long been expected to become increasingly apparent in observations as well, and there is now robust statistical and physical evidence of Antarctic ozone recovery (Kuttippurath & Nair, 2017; Solomon et al., 2016; Strahan & Douglass, 2018; Wang et al., 2025).

Although Antarctic ozone is expected to recover over time, the significance of recovery trends can be affected by different natural and anthropogenic processes (Kiesewetter et al., 2010; Stone et al., 2018; Weatherhead et al., 2000; Yook et al., 2022). The influence of different processes on ozone recovery has been extensively examined in previous studies, including the effects of volcanic eruptions (Hofmann & Oltmans, 1993; Ivy et al., 2017; Portmann et al., 1996; Solomon et al., 2016; Stocker et al., 2024), aerosols from Australian wildfires (Bernath et al., 2022; Solomon et al., 2022; Solomon et al., 2023), dynamical variability (Kiesewetter et al., 2010; Stone et al., 2018; Sweeney et al., 2025), the stratospheric temperature changes associated with different global warming scenarios (Karagodin-Doyennel et al., 2023), as well as supersonic aircraft emissions (Penner et al., 1999), and emissions from near-future rocket launches (Revell et al., 2025).

Modeling studies of nuclear war scenarios also suggest that even a limited regional conflict, such as an India-Pakistan scenario, could inject ~5 Tg of black carbon into the atmosphere and trigger substantial ozone depletion (Bardeen et al., 2021; Mills et al., 2014; Mills et al., 2008; Reisner et al., 2018; Yook et al., 2025). Previous studies have shown that this ozone loss is driven primarily by strong stratospheric warming caused by solar absorption by smoke particles (Bardeen et al., 2021; Mills et al., 2014; Mills et al., 2008) and is further enhanced by halogen emissions from large-scale urban fires burning chlorine- and bromine-containing materials following nuclear detonations, as well as by heterogeneous chemistry on smoke particles (Yook et al., 2025).

Here, we use a chemistry-climate model to examine how regional-scale nuclear wars in the late 21st century could affect the projected recovery of global, Arctic, and Antarctic ozone under declining stratospheric chlorine loading. This study builds on Yook et al. (2025) but with a different experimental design. Whereas previous simulations assumed present-day high-chlorine conditions and were limited to 3 years, here we investigate a nuclear war occurring after ozone recovery, under low background halogen loading over an extended 10-year simulation period. Section 2 describes the model and the different nuclear war emission scenarios. Section 3 examines the impacts of regional nuclear conflict on ozone recovery, and Section 4 provides a discussion and conclusions.

2. Data and methods

2.1. Model

We use the same version of the Whole Atmosphere Community Climate Model, version 4 (WACCM4;(Marsh et al., 2013), documented by Yook et al. (2025) to investigate climatic

138 responses to a regional nuclear conflict. We note that while the atmospheric component uses
139 WACCM4 from CESM1, the model is coupled to interactive ocean, land, and sea-ice
140 components from CESM2 (Danabasoglu et al., 2020). The model configuration has a horizontal
141 grid spacing of 1.9° × 2.5°, 66 vertical layers, and a model top near 140 km. The Model for
142 Ozone and Related Chemical Tracers (Kinnison et al., 2007) is used as the chemistry module.

143 Photolysis rates are calculated with the Tropospheric Ultraviolet and Visible radiation
144 scheme (Madronich & Flocke, 1997), which accounts for the influence of aerosol scattering and
145 absorption on actinic flux. Smoke aerosols are represented with the Community Aerosol and
146 Radiation Model for Atmospheres (CARMA; Bardeen et al., 2008). Following Yook et al.
147 (2025), this study incorporates updated stratospheric heterogeneous chemistry motivated by
148 wildfire observations and modeling that suggested enhanced HCl uptake on organic-rich smoke
149 aerosols (Solomon et al., 2023). These updates include enhanced HCl solubility in smoke
150 particles and the inclusion of smoke aerosol surface area in heterogeneous chemistry
151 calculations. Further details of the model setup and experimental design can be found in Bardeen
152 et al. (2021) and Yook et al. (2025).

153

154 **2.2. Model experiments**

155 The primary results are based on two sets of experiments conducted with WACCM4. The
156 first is a baseline future projection simulation (**CTRL**), in which greenhouse gas concentrations
157 follow historical values and Representative Concentration Pathway 6.0, while ozone-depleting
158 substance concentrations are prescribed according to the A1 scenario from Montzka et al. (2011).
159 This simulation is integrated from 2000 through the end of 2079.

The second set consists of nuclear war simulations representing a regional India-Pakistan (IP) conflict scenario, following Yook et al. (2025). These experiments are initialized from 1 January 2070 conditions in the **CTRL** simulation and integrated through the end of 2079. They include the following four emission scenarios:

1) The **IP-ALL** case is consistent with the **IP-ALL** case in Yook et al. (2025) and includes injections of ~6.7 Tg of smoke (5 Tg black carbon, BC, and 1.7 Tg organic carbon, OC), along with halogen emissions of 3 Tg chlorine and 0.08 Tg bromine. NO_x emissions from both the fireball and the fires are also included. All smoke particles and gases are injected over the India-Pakistan conflict region directly into the upper troposphere (150-300 hPa) during 12-15 January 2070,

2) The **IP** case is consistent with the **IP** case in Yook et al. (2025) and includes the same BC and OC emissions as the **IP-ALL** case, but without war NO_x and halogen emissions.

3) The **IP-ALL-5X-WIDE** case is similar to **IP-ALL** but uses five times larger war emissions and represents a broader conflict scale. In **IP-ALL-5X-WIDE** case, the emissions are not confined to the **IP** region, but are instead distributed homogeneously over a wider area spanning 20°S-20°N, and

4) The **IP-ALL-WIDE** is similar to **IP-ALL** case, except that the war emission area is broader as in **IP-ALL-5X-WIDE**.

Details of the war scenario and the associated aerosol and gas emissions are described in Toon et al. (2007), Bardeen et al. (2021), and Yook et al. (2025). All experiments use a single ensemble member. For simplicity, solar forcing is fixed at year 2000 values, and volcanic eruptions and prescribed QBO forcing are not included.

182

183 **2.3. Observations**

184 Observed ozone values for the 2000-2025 period were obtained from NASA Ozone
185 Watch and consist of Southern Hemisphere (SH) and Northern Hemisphere (NH) polar-cap total
186 column ozone averaged over latitudes poleward of 63° (http://ozonewatch.gsfc.nasa.gov).

187

188 **2.4. Analysis details**

189 Anomalies due to nuclear war emissions are defined as the difference between the
190 climate fields in the nuclear war simulations and those in the control simulation over the same
191 time period. Polar-cap averages are calculated over 63-90° in each hemisphere, consistent with
192 the NASA Ozone Watch definition of the polar cap.

193

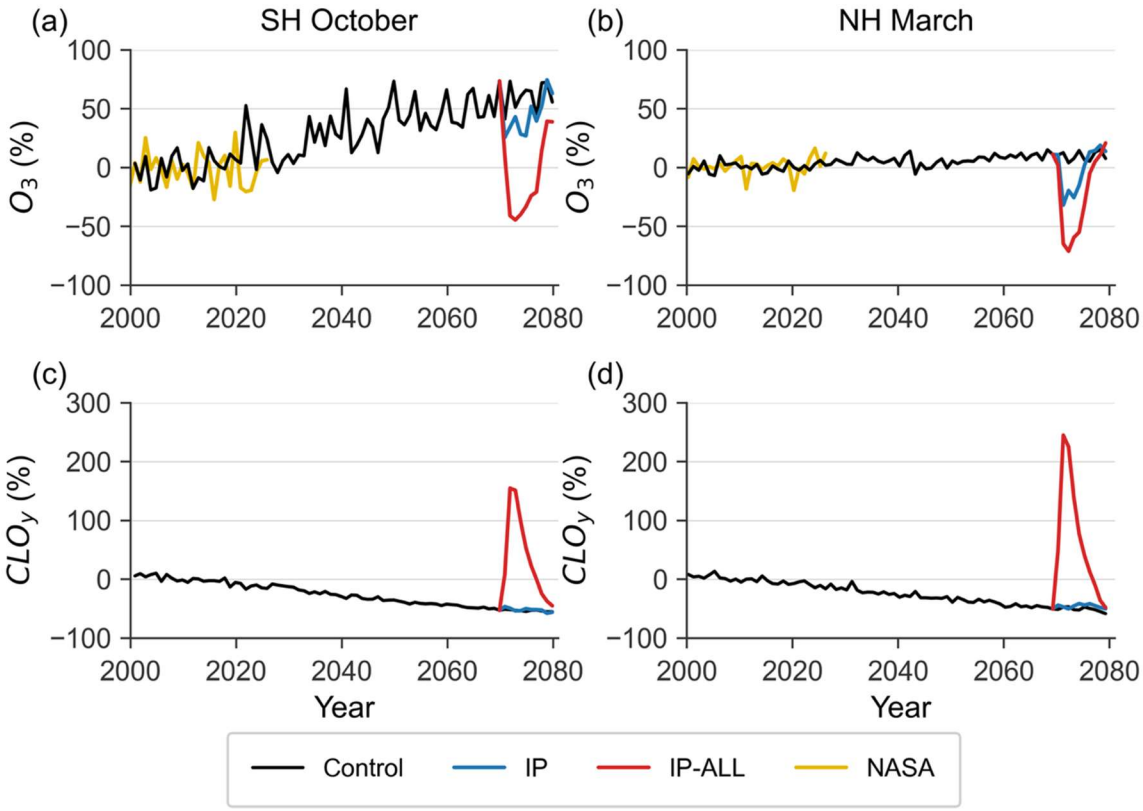

Figure 1. Time series of Southern Hemisphere (left) and Northern Hemisphere (right) polar-cap October total column ozone (O_3, % change in DU; top) and global stratospheric chlorine mass (ClO_y, % change in ppbv; bottom), respectively, from 2000 to 2080 for the control simulation (black), **IP** run (blue), and **IP-ALL** run (red).

3. Results

3.1. Projected ozone recovery in the 21st century

Figure 1 illustrates the expected recovery of ozone over the 21st century under declining stratospheric halogen loading and increasing greenhouse gases (GHGs). In the **CTRL** simulation (black line), polar-cap total column ozone increases markedly from the early 2000s onward, with trends of about 9.2% per decade (~20 Dobson Unit [DU] per decade) in the SH (Fig. 1a) and 1.6% per decade (~7 DU per decade) in the Northern Hemisphere (NH; Fig. 1b). By late century,

Antarctic ozone shows a recovery of over 50% relative to the 2000–2020 average, approaching its 1980 level (Figs. 1 and S1). While ozone recovery trends are sensitive to future emission scenarios (WMO, 2022; Karagodin-Doyennel et al., 2023), our **CTRL** run demonstrates an ozone recovery trend comparable to other WACCM4 simulations following different RCP scenarios (Figure S1).

The observations (yellow line) and **CTRL** simulation (black line) show broadly consistent interannual variability in SH October ozone during 2000–2025 (observations: $1\sigma = 33$ DU; CTRL: $1\sigma = 30$ DU after removing the linear trend). In contrast, NH March ozone observations show larger variability ($1\sigma = 30$ DU) than the model simulation ($1\sigma = 19$ DU). Notably, the ozone recovery over the 21st century is much larger than the year-to-year variability. A steady decline in stratospheric total inorganic chlorine loading is shown in both hemispheres, reflecting the long-term effects of the Montreal Protocol and its amendments (Figs. 1c-d). Overall, the results are consistent with the gradual healing of the Antarctic ozone hole as ozone-depleting substances decline and GHGs increase. Figures S1-2 shows the absolute changes in ozone (DU) and chlorine loading (ppbv), and the results are insensitive to whether they are expressed in relative (%) or absolute units.

3.2. Ozone loss in the late 21st century due to regional nuclear war

The **CTRL** simulation exhibits a robust and significant trend of ozone recovery. We next consider a regional nuclear war in the **IP** region occurring on 11 January 2070 to investigate its potential impacts on the projected ozone recovery (Fig. 1). In both hemispheres, the nuclear-war perturbation leads to a substantial amount of ozone loss. In the SH, October ozone drops from a late-century recovered state of roughly 60%-70% above the 2000-2020 baseline to about 20%

above it in the **IP** simulation (blue line in Fig. 1a), which includes only black carbon and organic carbon emissions, and to nearly 50% below the baseline level in the **IP-ALL** simulation (red line in Fig. 1a), which includes the same smoke emissions together with halogen emissions, essentially reopening the ozone hole. Similarly, in the NH, March ozone declines from about 10%-15% above baseline to roughly -30% in **IP** (blue line in Fig. 1b) and nearly -70% in **IP-ALL** (red line in Fig. 1b). Thus, halogen emissions substantially amplify the post-war peak ozone loss relative to smoke alone, producing a much deeper interruption of the projected ozone recovery.

The **CTRL** simulation also shows a robust declining trend in stratospheric background chlorine loading, reaching approximately 50% reduction compared to the 2000–2020 baseline by the end of the 2070s (Figs. 1c–d). In contrast, the **IP-ALL** scenario reveals the substantial impact of halogen emissions from nuclear war on stratospheric chlorine loading. Chlorine emissions from war-related fires are rapidly transported into the stratosphere, substantially elevating stratospheric chlorine loading above **CTRL** levels (Figs. 1c–d and S3b). Peak polar cap stratospheric chlorine loading in **IP-ALL** reaches ~4 ppbv in both hemispheres (Fig. S2), corresponding to roughly 150% and 250% increases over the 2000–2020 baseline in the SH and NH, respectively. These values are comparable to the levels of the early 1990s when chlorine loading was its peak. This elevated chlorine loading together with the high levels of organic aerosols resulting from the nuclear event drive enhanced halogen-catalyzed ozone losses. Thus, the results from Figure 1 collectively demonstrate that halogen emissions from urban fires linked to nuclear war substantially increase stratospheric chlorine loading and can lead to enhanced ozone losses. The detailed mechanisms underlying these halogen-driven ozone losses are examined in a later section (see also Fig. 5). We note that the **IP** scenario shows modest

254 troposphere-to-stratosphere chlorine transport associated with the smoke plume injection, though
255 substantially less than in **IP-ALL** (Figs. S3b-c).

256

257

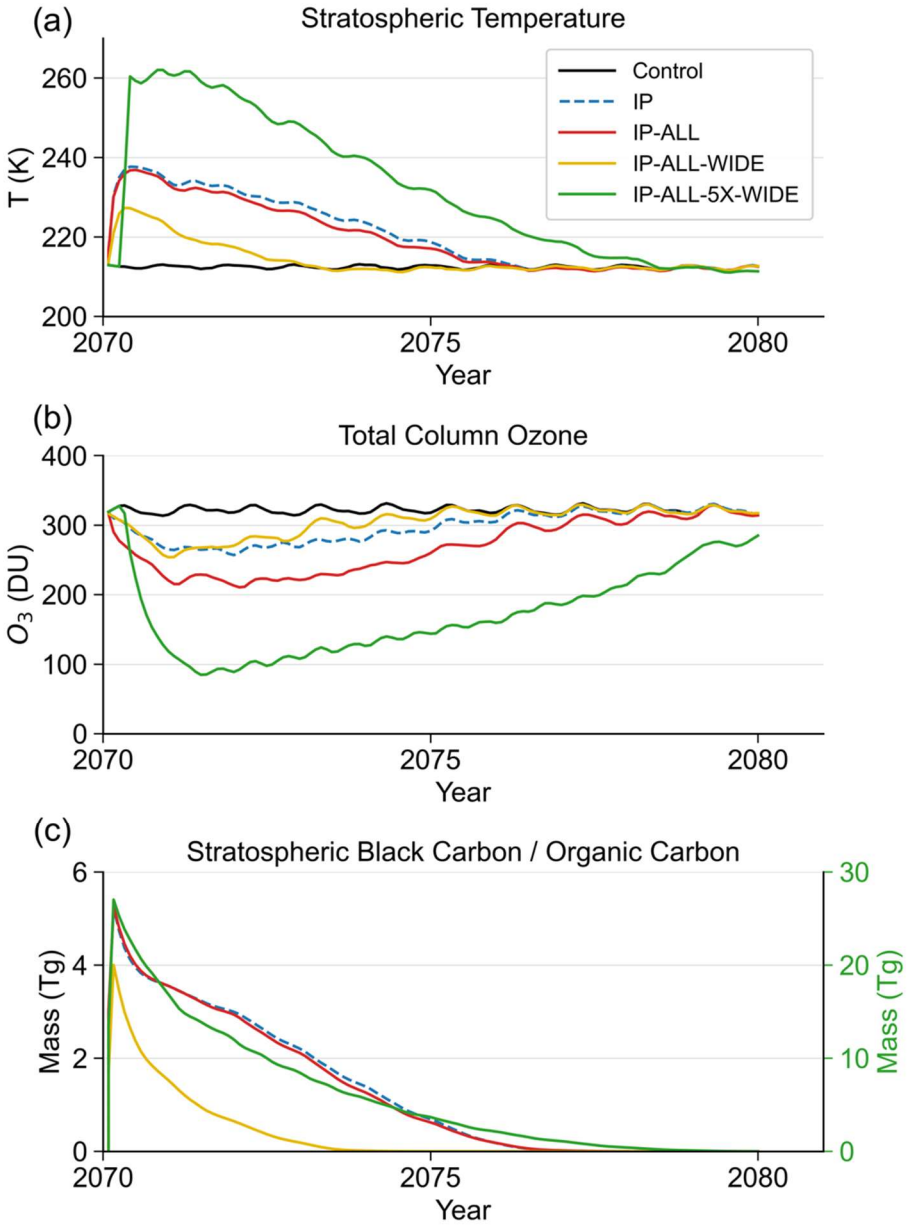

258

259 **Figure 2.** Time series of globally averaged (a) stratospheric temperature, (b) total column ozone, and (c)
260 stratospheric black carbon/organic carbon (BC/OC) mass for the **CTRL** (black), **IP** (blue), **IP-ALL** (red), **IP-**

ALL-WIDE (yellow), and **IP-ALL-5X-WIDE** (green) runs. "Stratospheric" denotes fields averaged from the tropopause to 1 hPa. In panel (c), the left y-axis shows the BC/OC mass for all scenarios except **IP-ALL-5X-WIDE**, while the right y-axis (green) displays the BC/OC mass for the **IP-ALL-5X-WIDE** scenario on an expanded scale to accommodate the substantially larger aerosol burden. Note that the time series is based on monthly data, so it includes the seasonal cycle. However, the solar cycle, volcanic eruptions, and QBO are not included in the simulation.

Figure 2 shows the time evolution of key atmospheric variables under different nuclear conflict scenarios, including stratospheric temperature, total column ozone, and stratospheric BC/OC mass. All scenarios produce stratospheric warming following the regional nuclear conflict, with magnitude varying by scenario. Both the **IP** (blue line) and **IP-ALL** (red line) runs, which include the same amount of smoke injection, produce peak stratospheric warming of ~25 K (Fig. 2a). This warming reflects the direct radiative heating from BC in the stratosphere (Robock et al., 2007). The **IP-ALL-5X-WIDE** scenario, representing 5 times larger emissions of smoke particles (25 Tg of BC), produces the most warming, reaching ~50 K. This enhanced warming in **IP-ALL-5X-WIDE** is consistent with the substantially larger war aerosol concentration and increased optical depth in the stratosphere.

All scenarios exhibit global ozone losses following the nuclear war, with the extent varying by emission scenario (Fig. 2b). The **IP** run produces peak total column ozone loss of ~60 DU (20%), while the **IP-ALL** scenario generates substantially greater depletion, reaching ~110 DU (35%) — in agreement with the peak ozone loss reported in **IP-ALL** in Yook et al. (2025) — indicating that war-related halogen emissions dramatically enhance ozone losses. The **IP-ALL-5X-WIDE** scenario exhibits the largest peak loss at ~240 DU (75%). Notably, ozone loss does not scale linearly with emission amount, consistent with results from sensitivity tests reported by Yook et al. (2025).

Next, we estimate the ozone recovery timescale. Ozone perturbations are defined here as the difference in ozone time series between 1) the control simulation and 2) the nuclear war simulations. We then calculate the linear trend of the ozone perturbations from the peak to December 2079. The recovery timescale is simply defined as the time required for ozone to recover to within a 4.5 DU threshold of the control, where this threshold corresponds to 1σ of ozone variability during the period of January 2070 to December 2079 in the **CTRL** run. Scenarios with smaller ozone loss — the **IP**, **IP-ALL**, and **IP-ALL-WIDE** runs — show recovery timescales of 6.4, 6.6, and 6.0 years, respectively. Thus, ozone in these runs recovers to near-control levels by 2075. However, the high-emission scenario, **IP-ALL-5X-WIDE**, exhibits a recovery timescale of 10.7 years and maintains significant ozone depletion through 2080.

The stratospheric BC/OC mass peaks in March 2070, followed by exponential decay in all runs (Fig. 2c). We estimate the e-folding timescale of the BC/OC time series simply as the time it takes to reach approximately 37% of the peak perturbation after applying a 12-month running mean to smooth the time series. The **IP**, **IP-ALL**, and **IP-ALL-5X-WIDE** scenarios show comparable e-folding timescales of 3.6, 3.4, and 2.8 years, respectively. In contrast, **IP-ALL-WIDE** exhibits a shorter decay timescale of 1.3 years. The sensitivity of stratospheric aerosol injection to emission density can be assessed by comparing the **IP-ALL** and **IP-ALL-WIDE** runs. The **IP-ALL** scenario (narrower emission region) implies more concentrated smoke injection compared to **IP-ALL-WIDE** (broader emission region), resulting in larger stratospheric warming (Fig. 2a) and enhanced plume rising, which leads to greater injection of the smoke plume higher into the stratosphere (Fig. 2c). These results suggest that emission density affects stratospheric smoke injection and the atmospheric lifetime of injected aerosols.

309 Figures 3 and 4 further explore the spatial patterns of total column ozone loss across
310 different emission scenarios. The **IP-ALL** run displays pronounced ozone depletion at high
311 latitudes in both hemispheres, with large ozone losses over the Arctic by the end of the first year
312 and over the Antarctic during austral spring months of the following year, with peak losses
313 exceeding 80% (Fig. 3a). Substantial ozone losses also occur at mid-latitudes in this scenario.
314 The pronounced Antarctic ozone losses are consistent with those observed in the current climate
315 under relatively high halogen loading, which creates more favorable conditions for ozone loss
316 due to cold temperatures and heterogeneous chemistry on PSC surfaces (Solomon, 1999). The
317 halogen emissions from nuclear war and heterogeneous chemistry on smoke particles contribute
318 to mid-latitude ozone loss (Yook et al., 2025).

319 The **IP** run also shows substantial ozone losses in both polar regions, but to a lesser
320 extent than **IP-ALL**, highlighting the enhanced ozone loss from halogen emissions in **IP-ALL**
321 (Fig. 3c). The **IP-ALL-WIDE** run exhibits smaller ozone losses despite the inclusion of halogen
322 emissions, due to reduced stratospheric smoke injection from the broader emission region, as
323 discussed in a previous section (Fig. 3b). The **IP-ALL-5X-WIDE** run demonstrates that
324 increasing total smoke mass amplifies ozone losses across all latitudes (Fig. 3d). In particular,
325 total column ozone is heavily depleted (>80%) at polar latitudes throughout the entire period,
326 highlighting the persistent ozone losses from such a high emission scenario.

327

328

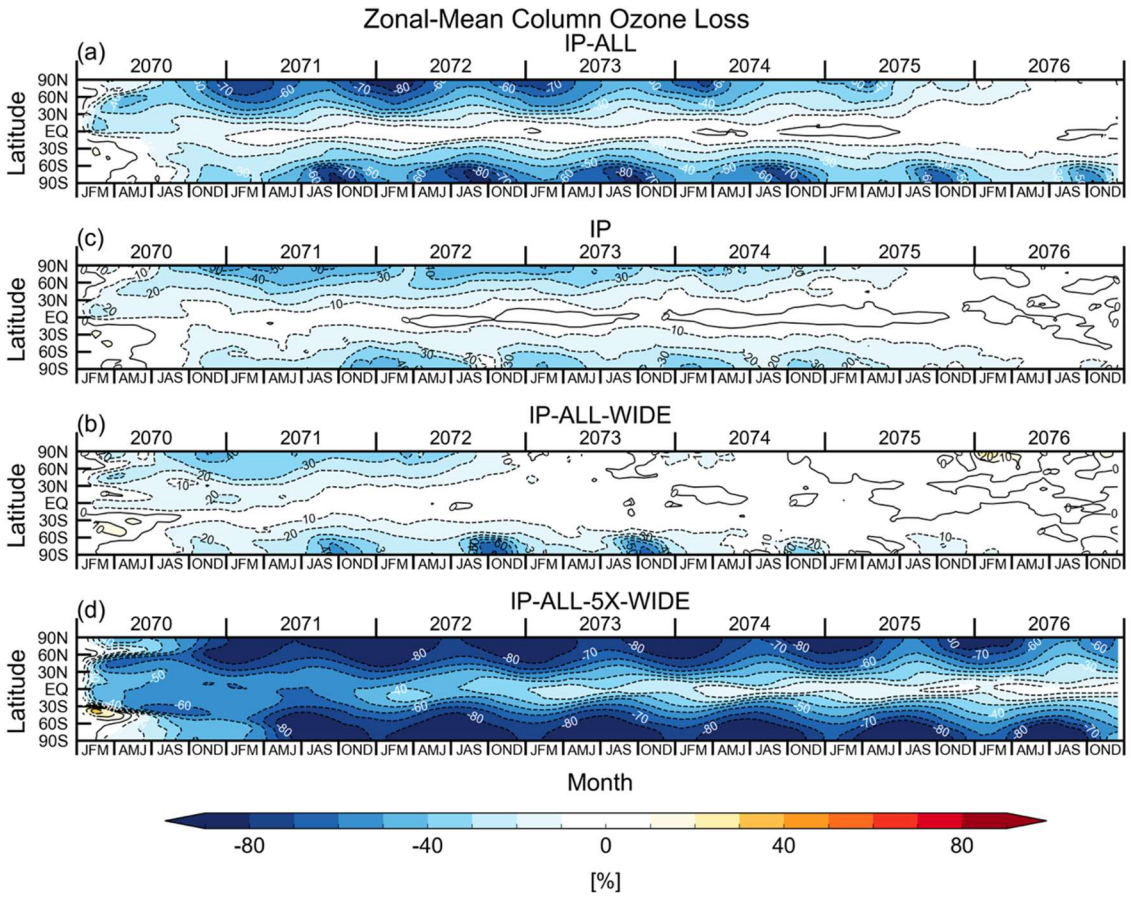

Figure 3. Zonal-mean percentage change in total column ozone relative to the **CTRL** run as a function of latitude and month for (a) **IP-ALL**, (b) **IP**, (c) **IP-ALL-WIDE**, and (d) **IP-ALL-5X-WIDE** runs.

The spatial distribution of total column ozone changes over polar regions in the NH (left panels, February–March average) and SH (right panels, October–November average) is shown in Figure 4. We compare ozone changes as the difference between two time periods: PRE (2000–2010) and POST (2070–2073), representing ozone recovery under declining halogen loading. The **CTRL** simulation shows modest ozone increases (~10%) across polar and mid-latitudes in the NH (Fig. 4a), but much higher increases (>80%) over the Antarctic (Fig. 4b), consistent with expected ozone recovery under the Montreal Protocol.

The **IP-ALL** simulation reveals changes in ozone relative to the **CTRL** PRE baseline, with losses reaching ~35% in the SH polar cap region (Fig. 4d) and exceeding 50% in the NH (Fig. 4c). In the SH, these losses exceed those associated with ozone holes in the early 21st-century climate represented by the **CTRL** PRE results, while the NH exhibits "Arctic ozone holes" characterized by substantial additional ozone losses over the Arctic. Figures 4e–f show the ozone losses from nuclear war during the POST period. More pronounced ozone losses occur over polar latitudes in both hemispheres, highlighting that nuclear war 1) disrupts the Antarctic ozone-hole recovery that would otherwise occur under the Montreal Protocol and 2) creates Arctic ozone holes as found in Yook et al. (2025).

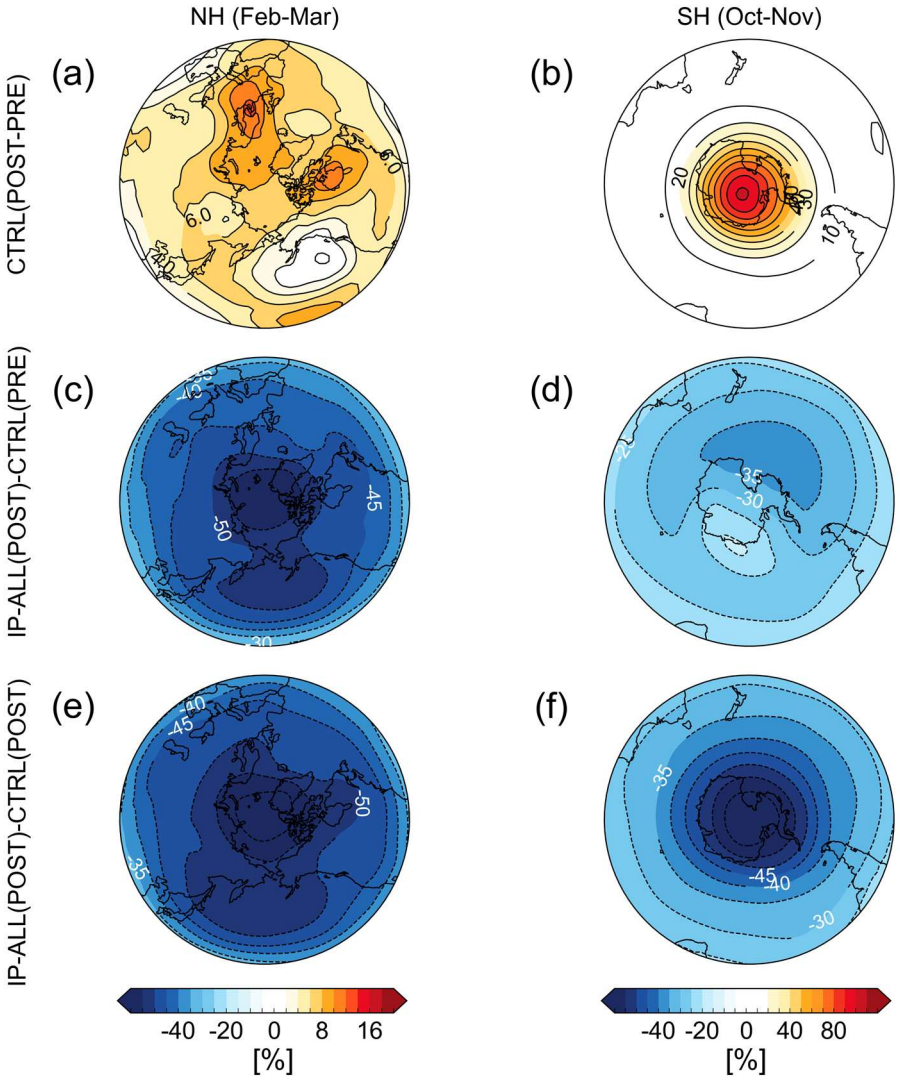

Figure 4. Percentage changes in total column ozone over the NH (left; February–March) and SH (right; October–November). Top panels (a–b) show **CTRL** run changes between the POST (2070–2073) and **PRE** (2000–2010) periods; middle panels (c–d) show **IP-ALL** POST-period ozone relative to the **CTRL** PRE baseline; and bottom panels (e–f) show IP-ALL ozone anomalies relative to **CTRL** during the POST period. Note that the color scales are non-linear and differ between hemispheres.

364 We evaluate the contribution of individual chemical pathways to ozone depletion by
365 tracking odd-oxygen loss rates, scaled by total odd-oxygen production, over 2070–2079 (Fig. 5).
366 Definitions of these production and loss terms are listed in Table 2 of Bardeen et al. (2021). In
367 the **IP-ALL** simulation, the ClO_x and BrO_x catalytic cycles increase substantially relative to the
368 **CTRL** simulation, whereas the NO_x catalytic cycle increases to a lesser extent and the HO_x cycle
369 decreases. This partitioning indicates that halogen chemistry is a primary driver of odd-oxygen
370 destruction in the **IP-ALL** simulation, consistent with Yook et al. (2025). Total column ozone
371 remains substantially reduced for about 6-7 years after the nuclear conflict (black solid line in
372 Fig. 5) before gradually recovering toward **CTRL** levels (black dashed line in Fig. 5). This
373 timescale corresponds closely to changes in halogen-catalyzed loss: ClO_x and BrO_x loss is
374 enhanced during the period of strongest ozone depletion and then declines as ozone begins to
375 recover.

376 These larger ozone losses in the **IP-ALL** simulation presented here and in Yook et al.
377 (2025), compared with previous simulations by Bardeen et al. (2021) and Mills et al. (2008) and
378 with the **IP** simulation without halogen emissions, are attributable to the combined nonlinear
379 effects of 1) additional halogen emissions from the nuclear war and 2) updated heterogeneous
380 chemistry on smoke particles. A detailed discussion of the role of halogen chemistry is provided
381 in Section 3.2 of Yook et al. (2025).

382

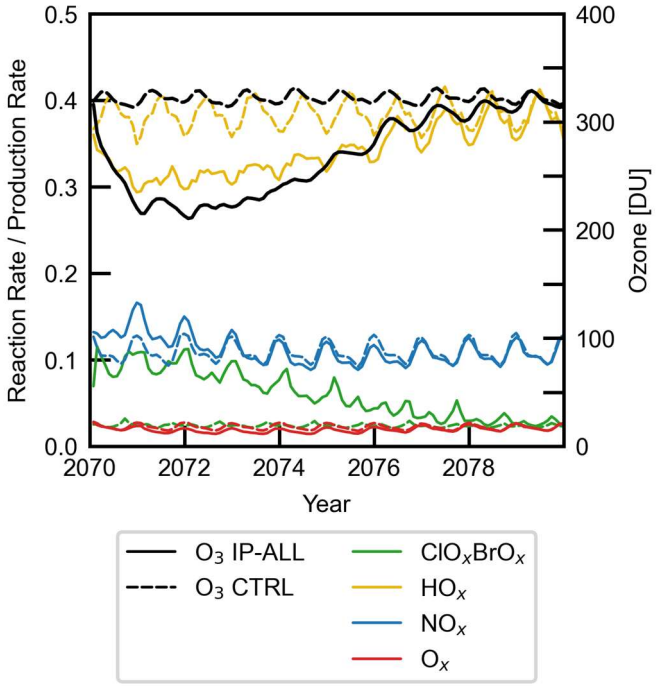

Figure 5. Evolution of total column ozone and column-integrated odd-oxygen loss rates relative to the total production rate of the respective case. Solid (dashed) lines denote results from the **IP-ALL** (**CTRL**) run.

4. Discussion and Conclusions

In this study, we used the chemistry-climate model WACCM4 to provide the first assessment of a regional nuclear conflict occurring in a *future state* in which the *ozone layer has substantially recovered*. Building on Yook et al. (2025), which examined a present-day India–Pakistan scenario under high background chlorine loading, we extended both the timing and duration of the analysis by simulating a nuclear conflict in 2070 — after ozone recovery under declining halogen loading — over a 10-year integration period. This experimental design allows

us to evaluate, for the first time, how such a conflict could disrupt the projected recovery of global stratospheric ozone in the mid-to-late 21st century.

Our baseline projection (**CTRL**) reproduces the expected healing of the ozone layer over the 21st century, with SH polar-cap total column ozone increasing at about 9% per decade as stratospheric chlorine declines under the Montreal Protocol and its amendments. Against this recovered background state, we find that a regional nuclear conflict could substantially reverse decades of ozone recovery. In the **IP-ALL** scenario, SH October ozone drops from a recovered state of 60–70% above the 2000–2020 baseline to nearly −50%, while NH March ozone declines to nearly −70%. These losses not only interrupt the projected recovery of the Antarctic ozone hole but also produce "Arctic ozone holes".

The importance of halogen emissions grows later in the 21st century as background stratospheric chlorine further declines. Comparison between the IP (smoke only) and **IP-ALL** (smoke plus halogens) scenarios shows that halogen emissions from urban fires substantially amplify ozone loss. The injection of stratospheric chlorine from nuclear war drives enhanced halogen-catalyzed ozone destruction, confirmed by our odd-oxygen budget analysis showing pronounced increases in the ClOx and BrOx cycles. The magnitude and persistence of ozone loss depend strongly on total amount of smoke emission. In the lower-emission scenarios (**IP**, **IP-ALL**, and **IP-ALL-WIDE**), ozone recovers to near-control levels within 6–7 years, whereas the high-emission **IP-ALL-5X-WIDE** scenario recovers over ~10 years and maintains significant ozone losses through 2080. We note that our results depend on assumptions regarding the quantity and composition of halogen and smoke emissions from urban fires as well as emission area and density, which remain uncertain and depend on the scale of the conflict and the

materials burned. Future work incorporating a broader range of emission scenarios would help constrain these uncertainties.

The resulting ozone depletion also leads to an increase in surface UV-B radiation that extends globally, including over highly populated mid-latitudes, and persists for several years (Bardeen et al., 2021; Yook et al., 2025). Because even short-term exposure to elevated UV radiation can have long-lasting health consequences (Slaper et al., 2001), these results point to potentially serious risks to human health — including higher skin-cancer mortality (Xu et al., in review) — that would linger long after the conflict itself. Regional nuclear conflicts are also projected to trigger multiple surface climate disruptions, including global cooling and reduced precipitation (Bardeen et al., 2021; Mills et al., 2014; Stenke et al., 2013; Toon et al., 2019; Yook et al., 2025).

In summary, our results demonstrate that even a regional nuclear conflict could inflict severe and long-lasting damage on the ozone layer, potentially reversing decades of global effort to heal it. This vulnerability increases as the ozone layer recovers and background chlorine declines, because halogen emissions from nuclear war constitute an increasingly dominant perturbation to a low-chlorine stratosphere. These findings underscore the far-reaching global consequences of nuclear conflict, which extend well beyond the regional scale to threaten the global climate, ecosystems, and human health.

Acknowledgments

S. S. and S. Y. were supported by a grant from the Future of Life Institute. The CESM project is supported primarily by the U.S. National Science Foundation. The authors

441 acknowledge the Climate Simulation Laboratory at NCAR's Computational and Information
442 Systems Laboratory (CISL; sponsored by NSF and other agencies) and the MIT's Massachusetts
443 Green High Performance Computing Center (supported by the Center for Sustainability Science
444 and Strategy) for providing computing and storage resources. Open Access funding enabled and
445 organized by MIT Hybrid 2026.

446

447

448

449

450

451

452

453

454

455

456

457

458

459

460

References

Bardeen, C., Kinnison, D. E., Toon, O. B., Mills, M. J., Vitt, F., Xia, L., et al. (2021). Extreme ozone loss following nuclear war results in enhanced surface ultraviolet radiation. *Journal of Geophysical Research: Atmospheres, 126*(18), e2021JD035079.

Bardeen, C., Toon, O., Jensen, E., Marsh, D., & Harvey, V. (2008). Numerical simulations of the three-dimensional distribution of meteoric dust in the mesosphere and upper stratosphere. *Journal of Geophysical Research: Atmospheres, 113*(D17).

Bernath, P., Boone, C., & Crouse, J. (2022). Wildfire smoke destroys stratospheric ozone. *Science, 375*(6586), 1292-1295.

Danabasoglu, G., Lamarque, J. F., Bacmeister, J., Bailey, D., DuVivier, A., Edwards, J., et al. (2020). The community earth system model version 2 (CESM2). *Journal of Advances in Modeling Earth Systems, 12*(2), e2019MS001916.

Dhomse, S. S., Kinnison, D., Chipperfield, M. P., Salawitch, R. J., Cionni, I., Hegglin, M. I., et al. (2018). Estimates of ozone return dates from Chemistry-Climate Model Initiative simulations. *Atmospheric Chemistry and Physics, 18*(11), 8409-8438.

Eyring, V., Waugh, D., Bodeker, G., Cordero, E., Akiyoshi, H., Austin, J., et al. (2007). Multimodel projections of stratospheric ozone in the 21st century. *Journal of Geophysical Research: Atmospheres, 112*(D16).

Farman, J. C., Gardiner, B. G., & Shanklin, J. D. (1985). Large losses of total ozone in Antarctica reveal seasonal ClO x/NO x interaction. *Nature, 315*(6016), 207-210.

Hofmann, D. J., & Oltmans, S. J. (1993). Anomalous Antarctic ozone during 1992: Evidence for Pinatubo volcanic aerosol effects. *Journal of Geophysical Research: Atmospheres, 98*(D10), 18555-18561.

Ivy, D. J., Solomon, S., Kinnison, D., Mills, M. J., Schmidt, A., & Neely III, R. R. (2017). The influence of the Calbuco eruption on the 2015 Antarctic ozone hole in a fully coupled chemistry-climate model. *Geophysical Research Letters, 44*(5), 2556-2561.

Jägermeyr, J., Robock, A., Elliott, J., Müller, C., Xia, L., Khabarov, N., et al. (2020). A regional nuclear conflict would compromise global food security. *Proceedings of the National Academy of Sciences, 117*(13), 7071-7081.

Karagodin-Doyennel, A., Rozanov, E., Sukhodolov, T., Egorova, T., Sedlacek, J., & Peter, T. (2023). The future ozone trends in changing climate simulated with SOCOLv4. *Atmospheric Chemistry and Physics, 23*(8), 4801-4817.

Keeble, J., Hassler, B., Banerjee, A., Checa-Garcia, R., Chiodo, G., Davis, S., et al. (2021). Evaluating stratospheric ozone and water vapour changes in CMIP6 models from 1850 to 2100. *Atmospheric Chemistry and Physics, 21*(6), 5015-5061.

Kiesewetter, G., Sinnhuber, B.-M., Weber, M., & Burrows, J. (2010). Attribution of stratospheric ozone trends to chemistry and transport: a modelling study. *Atmospheric Chemistry and Physics, 10*(24), 12073-12089.

Kinnison, D., Brasseur, G. P., Walters, S., Garcia, R., Marsh, D., Sassi, F., et al. (2007). Sensitivity of chemical tracers to meteorological parameters in the MOZART-3 chemical transport model. *Journal of Geophysical Research: Atmospheres, 112*(D20).

Kuttippurath, J., & Nair, P. J. (2017). The signs of Antarctic ozone hole recovery. *Scientific reports, 7*(1), 585.

MacKie, R. (2000). Effects of ultraviolet radiation on human health. *Radiation Protection Dosimetry, 91*(1-3), 15-18.

Madronich, S., & Flocke, S. (1997). Theoretical estimation of biologically effective UV radiation at the Earth's surface. In *Solar ultraviolet radiation: Modelling, measurements and effects* (pp. 23-48): Springer.

Madronich, S., Lee-Taylor, J. M., Wagner, M., Kyle, J., Hu, Z., & Landolfi, R. (2021). Estimation of skin and ocular damage avoided in the United States through implementation of the montreal protocol on substances that deplete the Ozone layer. *ACS Earth and Space Chemistry, 5*(8), 1876-1888.

Marsh, D. R., Mills, M. J., Kinnison, D. E., Lamarque, J.-F., Calvo, N., & Polvani, L. M. (2013). Climate change from 1850 to 2005 simulated in CESM1 (WACCM). *Journal of climate, 26*(19), 7372-7391.

Mills, M. J., Toon, O. B., Lee-Taylor, J., & Robock, A. (2014). Multidecadal global cooling and unprecedented ozone loss following a regional nuclear conflict. *Earth's Future, 2*(4), 161-176.

Mills, M. J., Toon, O. B., Turco, R. P., Kinnison, D. E., & Garcia, R. R. (2008). Massive global ozone loss predicted following regional nuclear conflict. *Proceedings of the National Academy of Sciences, 105*(14), 5307-5312.

Montzka, S., Reimann, S., Engel, A., Krüger, K., O'Doherty, S., Sturges, W., et al. (2011). Scientific Assessment of Ozone Depletion: 2010, Global Ozone Research and Monitoring Project. *WMO, Geneva, Switzerland, 516*.

Newman, P. A. (2018). The way forward for Montreal Protocol science. *Comptes Rendus. Géoscience, 350*(7), 442-447.

Oriowo, O. M., Cullen, A. P., Chou, B. R., & Sivak, J. G. (2001). Action spectrum and recovery for in vitro UV-induced cataract using whole lenses. *Investigative ophthalmology & visual science, 42*(11), 2596-2602.

Penner, J. E., Lister, D., Griggs, D. J., Dokken, D. J., & McFarland, M. (1999). *Aviation and the global atmosphere: a special report of the Intergovernmental Panel on Climate Change*: Cambridge University Press.

Portmann, R., Solomon, S., Garcia, R., Thomason, L., Poole, L., & McCormick, M. (1996). Role of aerosol variations in anthropogenic ozone depletion in the polar regions. *Journal of Geophysical Research: Atmospheres, 101*(D17), 22991-23006.

Reisner, J., D'Angelo, G., Koo, E., Even, W., Hecht, M., Hunke, E., et al. (2018). Climate impact of a regional nuclear weapons exchange: An improved assessment based on detailed source calculations. *Journal of Geophysical Research: Atmospheres, 123*(5), 2752-2772.

Revell, L. E., Bannister, M. T., Brown, T. F., Sukhodolov, T., Vattioni, S., Dykema, J., et al. (2025). Near-future rocket launches could slow ozone recovery. *npj Climate and Atmospheric Science, 8*(1), 212.

Robock, A., Oman, L., & Stenchikov, G. L. (2007). Nuclear winter revisited with a modern climate model and current nuclear arsenals: Still catastrophic consequences. *Journal of Geophysical Research: Atmospheres, 112*(D13).

Scherrer, K. J., Harrison, C. S., Heneghan, R. F., Galbraith, E., Bardeen, C. G., Coupe, J., et al. (2020). Marine wild-capture fisheries after nuclear war. *Proceedings of the National Academy of Sciences, 117*(47), 29748-29758.

Setlow, R. B. (1974). The wavelengths in sunlight effective in producing skin cancer: a theoretical analysis. *Proceedings of the National Academy of Sciences, 71*(9), 3363-3366.

Slaper, H., Matthijsen, J., den Outer, P., & Velders, G. (2001). Climatology of Ultraviolet Budgets Using Earth Observation (CUBEO): Mapping UV from the perspective of risk assessments.

Solomon, S. (1999). Stratospheric ozone depletion: A review of concepts and history. *Reviews of geophysics, 37*(3), 275-316.

Solomon, S., Dube, K., Stone, K., Yu, P., Kinnison, D., Toon, O. B., et al. (2022). On the stratospheric chemistry of midlatitude wildfire smoke. *Proceedings of the National Academy of Sciences, 119*(10), e2117325119.

Solomon, S., Garcia, R. R., Rowland, F. S., & Wuebbles, D. J. (1986). On the depletion of Antarctic ozone. *Nature, 321*(6072), 755-758.

Solomon, S., Ivy, D. J., Kinnison, D., Mills, M. J., Neely III, R. R., & Schmidt, A. (2016). Emergence of healing in the Antarctic ozone layer. *Science, 353*(6296), 269-274.

Solomon, S., Stone, K., Yu, P., Murphy, D., Kinnison, D., Ravishankara, A., & Wang, P. (2023). Chlorine activation and enhanced ozone depletion induced by wildfire aerosol. *Nature, 615*(7951), 259-264.

Stenke, A., Hoyle, C. R., Luo, B., Rozanov, E., Gröbner, J., Maag, L., et al. (2013). Climate and chemistry effects of a regional scale nuclear conflict. *Atmospheric Chemistry and Physics, 13*(19), 9713-9729.

Stocker, M., Steiner, A. K., Ladstädter, F., Foelsche, U., & Randel, W. J. (2024). Strong persistent cooling of the stratosphere after the Hunga eruption. *Communications Earth & Environment, 5*(1), 450.

Stone, K. A., Solomon, S., & Kinnison, D. E. (2018). On the identification of ozone recovery. *Geophysical Research Letters, 45*(10), 5158-5165.

Strahan, S. E., & Douglass, A. R. (2018). Decline in Antarctic ozone depletion and lower stratospheric chlorine determined from Aura Microwave Limb Sounder observations. *Geophysical Research Letters, 45*(1), 382-390.

Sweeney, A., Fu, Q., Solomon, S., Po-Chedley, S., Randel, W. J., Steiner, A., et al. (2025). Recent warming of the Southern Hemisphere subtropical lower stratosphere and Antarctic ozone healing. *AGU Advances, 6*(4), e2025AV001737.

Toon, O. B., Bardeen, C. G., Robock, A., Xia, L., Kristensen, H., McKinzie, M., et al. (2019). Rapidly expanding nuclear arsenals in Pakistan and India portend regional and global catastrophe. *Science Advances, 5*(10), eaay5478.

Toon, O. B., Robock, A., Turco, R. P., Bardeen, C., Oman, L., & Stenchikov, G. L. (2007). Consequences of regional-scale nuclear conflicts. In (Vol. 315, pp. 1224-1225): American Association for the Advancement of Science.

Wang, P., Solomon, S., Santer, B. D., Kinnison, D. E., Fu, Q., Stone, K. A., et al. (2025). Fingerprinting the recovery of Antarctic ozone. *Nature, 639*(8055), 646-651.

Weatherhead, E. C., Reinsel, G. C., Tiao, G. C., Jackman, C. H., Bishop, L., Frith, S. M. H., et al. (2000). Detecting the recovery of total column ozone. *Journal of Geophysical Research: Atmospheres, 105*(D17), 22201-22210.

Xia, L., & Robock, A. (2013). Impacts of a nuclear war in South Asia on rice production in mainland China. *Climatic Change, 116*(2), 357-372.

Yook, S., Solomon, S., Bardeen, C. G., & Stone, K. (2025). Arctic ozone hole and enhanced mid-latitude ozone losses due to heterogeneous halogen chemistry following a regional nuclear conflict. *Earth's Future, 13*(12), e2025EF006866.

Yook, S., Thompson, D. W., & Solomon, S. (2022). Climate impacts and potential drivers of the unprecedented Antarctic ozone holes of 2020 and 2021. *Geophysical Research Letters, 49*(10), e2022GL098064.

Journal of Geophysical Research: Atmosphere

Supporting Information for

Disruption of Ozone Recovery by Halogen Emissions from a Regional Nuclear Conflict

Simchan Yook[1]*, and Susan Solomon[1]

Affiliations:

[1] Department of Earth, Atmospheric and Planetary Sciences, Massachusetts Institute of Technology, Cambridge, MA, USA

Contents of this file

Figures S1 to S2

Introduction

This Supporting Information provides additional figures supporting the main-text analysis. Figures S1 (Figure. S2) reproduces Figs. 1a-b (Figs. 1c-d) but shows total column ozone in Dobson Units (stratospheric chlorine mass in Tg). Figure S1 also includes additional datasets from different model simulations and spans a longer period than Figure 1. Figure S3 presents the zonal-mean CLO_y concentration perturbations during the first year following the nuclear conflict (2070 annual mean) for the **IP-ALL** and **IP** scenarios relative to **CTRL**.

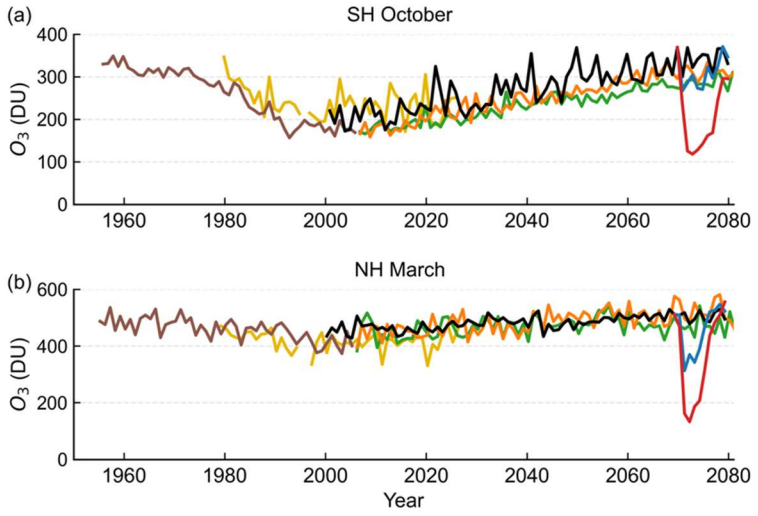

Figure S1. As in Figures 1a-b, but showing total column ozone in Dobson Units (DU) for (a) Southern Hemisphere October and (b) Northern Hemisphere March. This includes additional WACCM4 simulations from the CMIP5 project (Marsh et al., 2013): historical ensemble member 3 (1955–2005, brown), RCP4.5 ensemble member 3 (2005–2080, green), and RCP8.5 ensemble member 1 (2005–2080, orange).

Reference

Marsh, D. R., Mills, M. J., Kinnison, D. E., Lamarque, J.-F., Calvo, N., & Polvani, L. M. (2013). Climate change from 1850 to 2005 simulated in CESM1 (WACCM). Journal of climate, 26(19), 7372-7391.

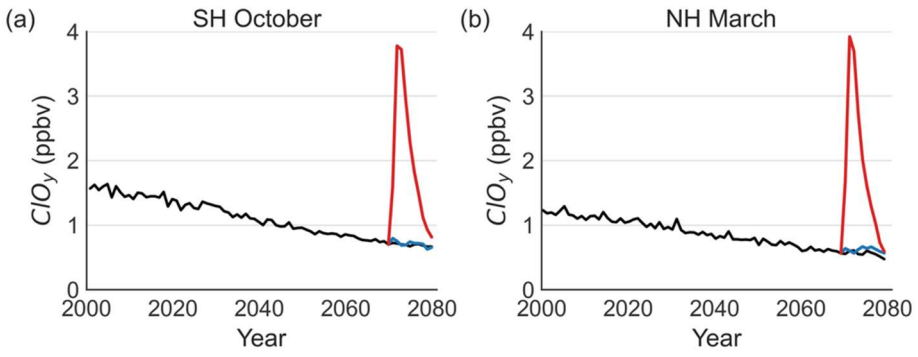

Figure S2. As in Figs.1c-d, but for stratospheric chlorine concentration in ppbv.

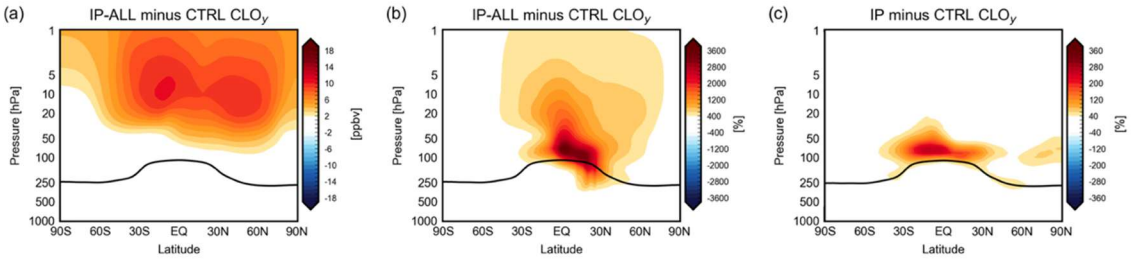

63

64 **Figure S3.** Zonal-mean CLO_y concentration perturbations during 2070. Shown are (a) **IP-**
65 **ALL** minus **CTRL** in absolute volume mixing ratio (ppbv), (b) **IP-ALL** minus **CTRL** in
66 percentage anomaly (%), and (c) **IP** minus **CTRL** in percentage anomaly (%). The black
67 line indicates the tropopause height from the **IP-ALL** simulation.

68

69

70

71